frontiers | Frontiers in Materials

TYPE Original Research
PUBLISHED 15 April 2025
DOI 10.3389/fmats.2025.1566490

OPEN ACCESS

EDITED BY
Vineet Kumar,
Yeungnam University, Republic of Korea

REVIEWED BY
Ande Fudja Rafryanto,
Nano Center Indonesia, Indonesia
Sakshi Kabra Malpani,
Save The Water, United States
Nassima Meftah,
El-Oued University, Algeria

*CORRESPONDENCE
Gemechu Deressa Edossa,
gemechu.deressa@astu.edu.et
Fedlu Kedir Sabir,
fedluked130@gmail.com

RECEIVED 24 January 2025
ACCEPTED 03 March 2025
PUBLISHED 15 April 2025

CITATION
Muhammud AM, Edossa GD and Sabir FK (2025) High-performance nanostructured SiO_2 from Ethiopian pumice: synthesis and characterization.
Front. Mater. 12:1566490.
doi: 10.3389/fmats.2025.1566490

High-performance nanostructured SiO_2 from Ethiopian pumice: synthesis and characterization

Agraw Mulat Muhammud, Gemechu Deressa Edossa* and Fedlu Kedir Sabir*

Department of Applied Chemistry, College of Applied Natural Science, Adama Science and Technology University, Adama, Ethiopia

The increasing demand for high-performance, cost-effective nanomaterials has driven significant interest in utilizing natural resources for advanced material production. This study presents the synthesis of nanostructured SiO_2 from Ethiopian pumice through a sustainable, environmentally friendly, and cost-effective green chemistry approach. The process involved pumice purification and beneficiation, followed by alkaline leaching and wet sol–gel precipitation, achieved with low energy input and without the need for ablation or post-grinding steps. The end product's properties were comprehensively analyzed using various techniques, including atomic absorption spectroscopy (AAS), X-ray diffraction (XRD), Fourier transform infrared spectroscopy (FTIR), thermal analysis (TGA), UV-is spectroscopy, Brunauer–Emmett–Teller (BET) analysis, dynamic light scattering (DLS), scanning electron microscopy (SEM), and energy dispersive X-ray analysis (EDAX). AAS and EDAX analyses confirmed a high purity of 98.52% and an overall yield of 69.07%, within the upper range (50%–75%) reported in the literature, indicating a well-optimized process. BET analysis showed an average pore size of 86.63 nm along with a significant specific surface area of 571.48 m^2/g. FTIR identified silanol (Si–OH) and siloxane (Si–O–Si) groups, while XRD revealed an amorphous structure. TGA demonstrated enhanced thermal stability up to 900°C, and UV–Vis analysis verified optical purity. DLS analysis revealed a uniform hydrodynamic diameter distribution within the favorable 10–100 nm range, while SEM images indicated an average primary particle size of 35.83 nm. This study optimized the synthesis of high-purity zero-dimensional (0D) nanostructured SiO_2 from Ethiopian pumice, achieving uniform particle size, high surface area, and enhanced stability. The resulting 0D SiO_2 outperforms conventional sources in both structural and functional properties, aligning with existing literature and industry standards and positioning it as an ideal and highly effective reinforcement filler for rubber composites. Its versatile properties also support applications in catalysis, adsorption, coatings, and optoelectronics. This work highlights Ethiopian pumice as a sustainable, cost-effective source of advanced silica materials with a strong potential for import substitution in Ethiopia's tire industry.

KEYWORDS

nanostructured SiO_2, Ethiopian pumice, sustainable synthesis, material characterization, rubber composite reinforcement

1 Introduction

Global industries face challenges related to outdated technologies, limited access to raw materials, and rising input costs. Nanomaterials have emerged as a promising solution to mitigate these issues (Roco and Bainbridge, 2002). Among these materials, nanostructured silica has emerged as significant attention due to its unique nanoscale characteristics, including small particle size, high uniformity, superior stability, and surface-active characteristics (Li et al., 2012), making it highly versatile for applications in rubber (Muhammud and Gupta, 2022), catalysis (Song et al., 2020), adsorption (Dizgeet, 2022; Wang, 2019; Hani et al., 2023), coatings (Beneditt-Jimenez et al., 2022), and electronics (Laskowski et al., 2019; Shimomura, 2023). Nanostructured silica, in particular, enhances mechanical strength, thermal stability, and abrasion resistance in tire rubber composites, contributing to fuel-efficient and high-performance green tires (Thirumalai et al., 2017; Zhang et al., 2020; Wang, 2018).

The growing demand for high-performance and cost-effective nanomaterials has intensified research into sustainable sources for synthesizing silica. Traditional methods often rely on synthetic precursors such as tetraethyl orthosilicate (TEOS) and energy-intensive processes, leading to high costs and environmental concerns. Addressing these challenges requires the development of eco-friendly, cost-effective, and scalable synthesis routes that utilize natural and abundant raw materials. While nanostructured silica can be derived from various biogenic sources, including rice husk (Zhang et al., 2014), corn cobs (Adam, 2011), teff straw (Gebretatios and Raghavan, 2021), and wheat husk (Kumar, 2017), as well as mineral sources like olivine (Rønning, 2004), perlite (Demir et al., 2019), silica sand (Aziz, 2014), granite (Santhosh et al., 2016), clay (Zhang, 2012), and diatomaceous earth (Zhao, 2015a), the search for more sustainable and cost-effective raw materials remains a critical challenge (Zhang, 2021; Pereira, 2018).

Pumice rock, formed through volcanic activity, is lightweight, porous, and rich in silica, along with other oxides like Al_2O_3 and Fe_2O_3 (Kumar and Prakash, 2019). Widely used in construction and filtration in various parts of the world, including Africa (Ravindra, 2021), its potential for high-value nanomaterial production remains underexploited (Günkaya and Banar, 2018). Ethiopian pumice, which is abundant, cost-effective, and composed of 60%–70% amorphous silica (Mulugeta and Tadesse, 2018; Kebede, 2020), offers a promising alternative for nanostructured silica synthesis (Ravindra, 2021; Ogunbiyi et al., 2019).

Currently, Ethiopia imports various grades of nanostructured silica for use in tire rubber, paints, printing inks, and plastics (Geda and Shimeles, 2007). While biomass-derived silica has shown potential in Ethiopia, one study (Bageru and Srivastava, 2018) successfully extracted nanostructured silica from teff straw ash for use as biocomposites with chitosan and alginate for pyridine removal.

Similarly, another study (Jembere, 2017) explored the potential of rice husk ash-derived silica in rubber tread compounds at Horizon Addis Tire Factory as a substitute for imported commercial silica. While these studies have shown promise, they involve multiple processing steps, such as seasonal biomass collection, an ablation step to produce ash, and additional grinding before application, limiting their economic feasibility.

In contrast, Ethiopia has abundant pumice rock, containing 60%–70% amorphous silica, with approximately 800,000 metric tons mined in 2019 (Crangle, 2019). Unlike biogenic sources, pumice is a scalable and energy-efficient option for nanostructured silica production, requiring no ablation or post-grinding and free of seasonal collection limits.

Compared to conventional energy-intensive and less environmentally friendly silica production, recent research prioritizes cost-effective and sustainable extraction from siliceous mineral ores like pumice. The synthesis of nanostructured silica can be achieved through various methods, each differing in scalability, energy efficiency, product purity, and industrial applicability. Hydrothermal synthesis utilizes high-temperature aqueous solutions to produce crystalline silica with controlled particle size; however, it is energy-intensive, requires high pressure, and faces scalability limitations and environmental challenges (Kumar, 2019; Mohammed et al., 2021). Microwave-assisted synthesis (Zhao, 2015b; Imoisili and Jen, 2022) and flame synthesis (Wang, 2018) enhance energy efficiency and scalability but present challenges related to equipment requirements and particle uniformity. Solvothermal synthesis (Lee, 2014), while achieving superior purity, remains costly and impractical for large-scale production. Acid–base precipitation is a simpler, cost-effective method but struggles with controlling particle size and morphology, and the use of strong acids and bases poses environmental concerns (Manurung et al., 2022).

Among the various methods, the sol–gel process is a versatile and environmentally friendly technique for efficiently extracting and converting pumice into high-performance nanostructured silica. Operating under mild conditions, it allows precise control over silica morphology and surface area while reducing energy consumption and minimizing the need for harsh chemicals, aligning with green chemistry principles (Brinker and Scherer, 1990).

Its scalability and ability to produce high-purity silica with tailored properties make it ideal for industrial applications (Kumar, 2019). In this study, an optimized alkaline leaching-sol–gel method incorporating controlled washing, drying, and calcination was identified as the most efficient and sustainable approach for producing high-performance nanostructured silica from pumice, modifying methods from previous research (Kumar, 2019; Mulugeta and Tadesse, 2018). This method lowers production costs while enhancing environmental sustainability, making it industrially viable (Karande et al., 2021; Emrie, 2024).

Ethiopian pumice, a silica-rich volcanic glass, represents an abundant yet underutilized resource for the synthesis of high-performance nanostructured silica. Despite its high silica content, the potential of Ethiopian pumice in nanomaterial synthesis remains largely unexplored. This study addresses this gap by extracting and synthesizing nanostructured silica from Ethiopian pumice through a systematic process involving purification, alkaline leaching, and sol-gel precipitation. The adopted method aligns with green chemistry principles by minimizing the use of toxic solvents and harsh chemicals while maintaining mild synthesis conditions to ensure sustainability and scalability. Comprehensive characterization revealed the structural, morphological, and thermal properties of the synthesized silica.

A key motivation for this study is the potential industrial application of the synthesized silica material, which has been

evaluated and identified as an ideal reinforcement filler for rubber composites. The tire industry, in particular, depends on high-performance silica fillers to enhance mechanical strength, abrasion resistance, thermal stability, and rolling efficiency. This material demonstrates strong potential for import substitution in Ethiopia's tire industry. Additionally, this study promotes the utilization of local resources that reduce production costs and support sustainable industrial development while contributing to global advancements in materials science and environmental sustainability.

2 Materials and methods

2.1 Materials

2.1.1 Chemicals

The chemicals for the synthesis of high-performance nanostructured SiO_2 from Ethiopian pumice were sourced from local chemical suppliers in Addis Ababa and used as received without further purification. Analytical-grade sodium hydroxide (99% purity, NaOH) was utilized for the preparation of Na_2SiO_3 solutions derived from pumice digestion and maintaining the alkalinity of different solutions. Analytical-grade sulfuric acid (H_2SO_4) from Merck (Germany) was employed as a 5 M solution prepared from concentrated acid (98% purity) for neutralizing the sodium silicate solution to form SiO_2 gel from sodium silicate. Hydrochloric acid (HCl), analytical grade, procured from BDH Chemicals (United Kingdom), was used as a 1 M solution prepared from concentrated HCl (37% purity) for removing impurities from the prepared SiO_2 nanostructure. Deionized water (DI water), laboratory-grade, sourced from an in-house purification system, was used throughout the synthesis. Analytical-grade ethanol (99.9% purity, C_2H_5OH), obtained from Fisher Scientific (United States), served as a solvent in the washing process and solution preparation.

2.1.2 Equipment

The equipment used in the synthesis and characterization process included a magnetic stirrer, hot plate, beakers, pH meter, vacuum filtration setup, oven, centrifuge, muffle furnace, analytical balance, mortar and pestle, three-neck round-bottom flask with reflux setup, crucibles, jaw crusher, electric grinder, thermometer, Whatman filter paper, and aluminum foil.

2.2 Experimental procedures

2.2.1 Collection, beneficiation, and characterization of pumice

Following consultation recommendations from the Geological Survey of Ethiopia, the Ethiopian pumice rock used in this study, with a silica content of 64.82%, was collected from the Tatek quarry in the Rift Valley region, owned by the Mugher Cement Factory. The pumice, selected for its high silica content, was originally intended for cement production.

The beneficiation and purification of pumice were carried out based on a baseline study (Sarikaya et al., 2017), with modifications made to increase its silica concentration, quality, and usability by removing impurities before using it as a precursor for SiO_2 nanostructure preparation as shown in Figure 1. Initially, the collected pumice was cleaned through a multi-step wash with distilled water to remove dust, debris, and soluble contaminants. It was then oven-dried at 100°C for 12 h to eliminate moisture, cooled, and crushed using a jaw crusher. The crushed pumice was ground into finer particles with an electric grinder and sieved through a 180-μm mesh to ensure uniform particle size. The sieved pumice was subjected to calcination at 500°C for 4 h, resulting in the formation of meta-pumice. After calcination, the material was comprehensively analyzed for its properties, including optical behavior (UV–Vis spectroscopy), thermal stability (TGA), particle size distribution (DLS), surface texture and elemental composition (SEM-EDAX), phase identification (XRD), functional groups (FTIR), pore structure and specific surface area (BET), and silicate content and elemental concentration (AAS). The purified and characterized material was subsequently used as a precursor for SiO_2 extraction.

FIGURE 1
Provides a pictorial representation of the beneficiation process of Ethiopian pumice.

2.2.2 Synthesis of 0D nanostructured SiO_2

The beneficiated and purified Ethiopian pumice powder was utilized as a precursor for the synthesis of 0D nanostructured SiO_2 under optimized conditions established in an unpublished study. Key synthesis parameters, including temperature, reaction time, pH, and reagent concentrations, were carefully monitored to achieve the desired properties. Nanostructured SiO_2 was synthesized following a modified procedure based on a typical

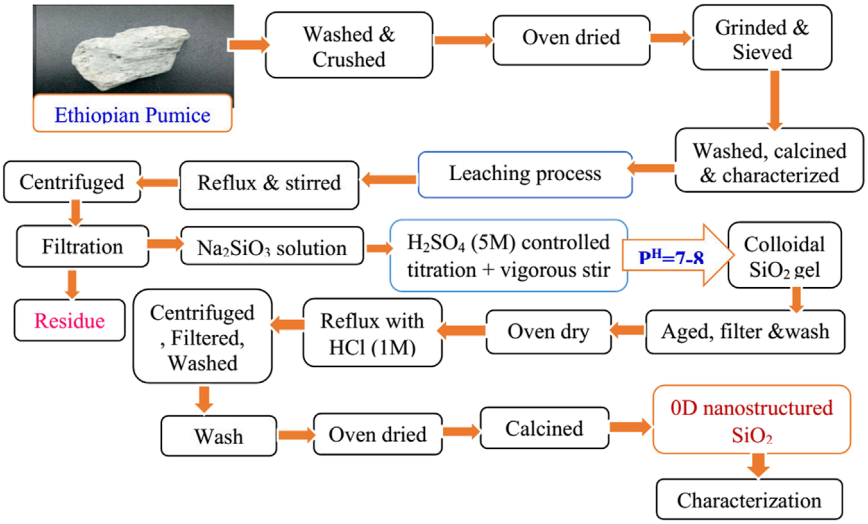

FIGURE 2
Presents the complete sol–gel process flowchart for the synthesis of 0D nanostructured SiO_2 from pumice.

experimental approach as shown in Figure 2 (Mourhly et al., 2015). Initially, 30 g of pumice powder was dispersed in 300 mL of 3 M NaOH within a three-neck round-bottom flask and refluxed at 90°C for 2 h and 30 min to form a sodium silicate solution as shown in Figure 3. The resulting solution was centrifuged, filtered, and washed with minimal amounts of boiling distilled water.

After cooling, 5 M H_2SO_4 was added dropwise to titrate the sodium silicate solution. During the reaction between Na_2SiO_3 and H_2SO_4 in the presence of water, soluble silica ($Si(OH)_4$) sol and sodium sulfate (Na_2SO_4) were formed as shown in Figure 4. The pH of the solution was maintained at 7–8 to facilitate the formation of an SiO_2 gel, which was stirred continuously for 30 min.

The gel was then aged at room temperature for 24 h to enhance uniformity and morphology before being filtered, washed, and dried at 80°C for 24 h. To remove residual soluble minerals, the dried SiO_2 was refluxed with 1 M HCl at 100°C for 3 h, followed by centrifugation, filtration, and oven drying at 120°C for 12 h. Finally, the purified SiO_2 was calcined at 600°C for 5 h to eliminate organic residues, following a modified protocol adapted from similar studies (Pereira, 2018; Karande et al., 2021; Emrie, 2024).

The overall chemical reactions involved in the alkaline extraction of the sodium silicate solution from Ethiopian pumice, followed by the sol–gel synthesis of SiO_2 nanostructures, are presented below. These reactions have been adapted from a similar study (Mourhly et al., 2015) with significant modifications:

$$NaOH + Pumice \rightarrow Na_2SiO_3\,(solution),$$

$$2Na_2SiO_3 + 2H_2O + 2H_2SO_4 \rightleftharpoons 2Si\,(OH)_4\,(sol) + 2Na_2SO_4$$

$$Na_2SiO_3 + H_2SO_4 \rightarrow SiO_2\,gel\,(at\ pH\ 7-8).$$

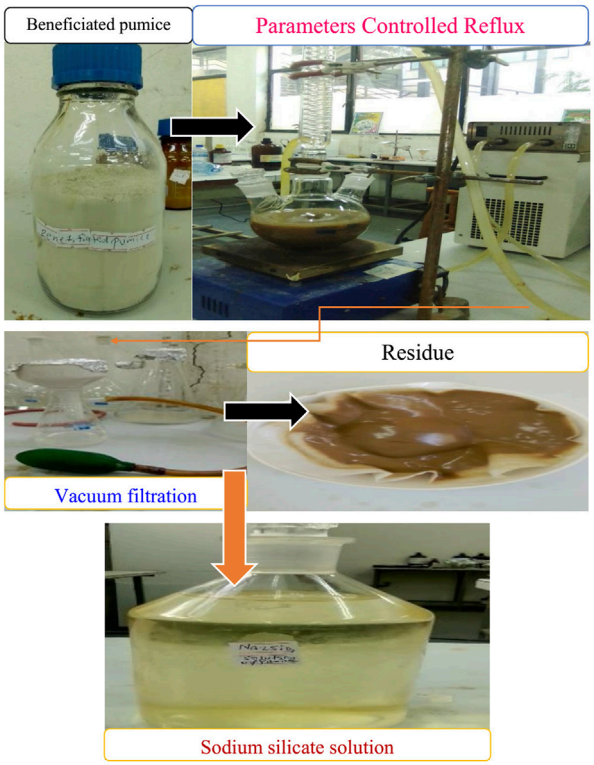

FIGURE 3
Shows the alkaline leaching of pumice.

2.2.3 Characterization of 0D nanostructured SiO_2

The high-performance nanostructured SiO_2 synthesized from Ethiopian pumice was comprehensively characterized using

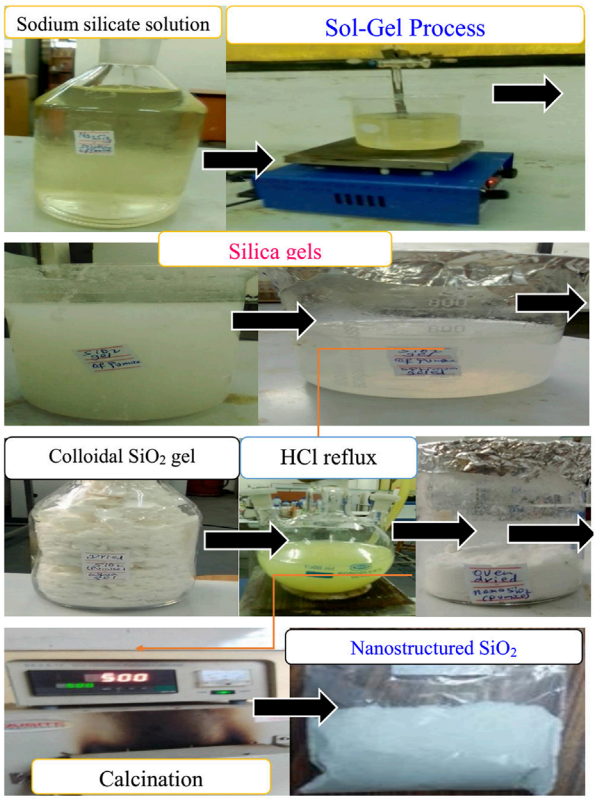

FIGURE 4
Illustrates the sol–gel process for preparing nanostructured SiO_2.

advanced analytical techniques. Atomic absorption spectroscopy (AAS) was employed to determine the elemental composition, while X-ray diffraction (XRD) was used to analyze the crystalline structure and phase purity. Additional tailored properties were investigated as follows: thermal stability using thermogravimetric analysis (TGA), optical properties via UV–Vis spectroscopy, particle size distribution by dynamic light scattering (DLS), functional groups identified through Fourier transform infrared (FTIR) spectroscopy, surface area and pore size measured by Brunauer–Emmett–Teller (BET) analysis, and surface morphology, particle size, and elemental composition examined using scanning electron microscopy with energy dispersive X-ray spectroscopy (SEM-EDAX).

3 Results and discussion

3.1 Chemical composition analysis

The atomic absorption spectroscopy (AAS) analysis of silicate content, conducted at the Ethiopian Geological Survey Laboratory and presented in Table 1, confirmed a substantial increase in silica purity from 64.82% in beneficiated pumice to 98.52% in the synthesized nanostructured SiO_2. This remarkable improvement confirms the effective removal of major impurities such as Al_2O_3 and Fe_2O_3, along with other minor oxide contaminants typically found in natural pumice. The synthesized nanostructured SiO_2 exhibits superior purity compared to previous studies, which reported purity levels of 94% (Mourhly et al., 2015), 94.44% (Mourhly et al., 2019), 86.8% (Raza, 2019), 96.83% (Imoisili et al., 2020), and 93.299% (Hidayah, 2024), and is comparable to the 99% reported by Alves et al. (2017). The decrease in loss on ignition (LOI) from pumice to nanostructured SiO_2 confirmed a reduction in impurity and moisture levels. The chemical compositional analysis showed that the purity level of nanostructured silica synthesized from Ethiopian pumice is similar to that of commercially produced silica, which is usually obtained through expensive and complex processes.

Standard commercial silica, used in rubber, glass, or coatings, typically has a purity range of 95%–99%. These results suggest that the nanostructured silica from Ethiopian pumice can be a sustainable and cost-effective alternative to high-grade commercial silica, making it suitable for high-performance applications like rubber reinforcement, catalysis, and electronics. The presence of alkali metal and alkaline earth metal oxides in small amounts does not significantly impact the performance of silica for the intended applications in our study.

3.2 Structural properties from XRD

X-ray diffraction (XRD) analysis, presented in Figure 5, confirms phase transformations in the Ethiopian beneficiated pumice during the synthesis of nanostructured silica. The XRD pattern of the beneficiated pumice reveals sharp peaks at $2\theta = 27°$, indicating the presence of crystalline silica and metal oxides, such as quartz (Rampe et al., 2023), consistent with natural SiO_2 phases in pumice.

Additional impurity peaks at $2\theta \approx 30°$, 50°, and 60° correspond to residual crystalline phases of materials like Fe_2O_3 and Al_2O_3, with notable peaks at $2\theta \approx 25.6°$, 35.1°, and 43.4° for Al_2O_3 (corundum) and peaks at $2\theta \approx 29.0°$ and 33.0° for Na_2O (Hidayah, 2024). In contrast, the XRD pattern of the pumice-derived nanostructured SiO_2 exhibits a broad hump centered approximately 20°–30° 2θ, characteristic of amorphous silica (Rønning, 2004; Bachir et al., 2023; Luthfiah et al., 2021), which is typical for sol–gel-synthesized SiO_2. Minor residual peaks, resulting from trace amounts of crystalline silica or other impurities of alkali metal oxides, are observed at low intensities, confirming the predominance of an amorphous SiO_2 structure (Mourhly et al., 2019; Khattak et al., 2023), validating purity and the successful synthesis of nanostructured SiO_2. This transition from a crystalline to an amorphous state enhances surface area and reactivity, making the synthesized nanostructured SiO_2 suitable for applications such as rubber reinforcement, adsorption, and catalysis.

3.3 Functional groups identified by FTIR

FTIR analysis (Figure 6) shows the structural transformation of beneficiated pumice into high-purity nanostructured SiO_2, emphasizing its enhanced reactivity. The FTIR spectrum of beneficiated pumice exhibits characteristic peaks at 3,700–3,200 cm^{-1} (O–H stretching of water molecules) and a sharp absorption band at approximately 3,750 cm^{-1} due to isolated

10.3389/fmats.2025.1566490

TABLE 1 Complete silicate analysis report of beneficiated pumice and pumice-derived nanostructured SiO_2 by AAS.

Collector's code	SiO_2	Al_2O_3	Fe_2O_3	CaO	MgO	Na_2O	K_2O	MnO	P_2O_5	TiO_2	H_2O	LOI
Beneficiated pumice	64.82	16.40	2.68	2.48	0.36	3.06	3.00	0.10	0.13	0.21	1.30	5.46
Pumice nano SiO_2	98.52	0.252	0.252	0.02	0.10	0.12	0.110	<0.01	0.09	<0.01	0.02	0.37

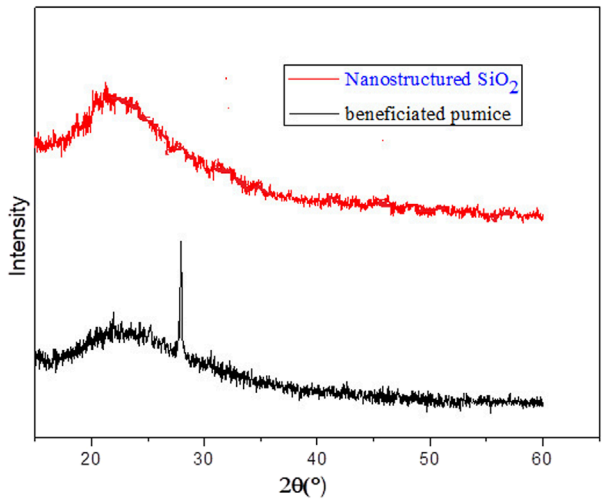

FIGURE 5
Displays the X-ray diffractograms of beneficiated pumice and pumice-derived SiO_2.

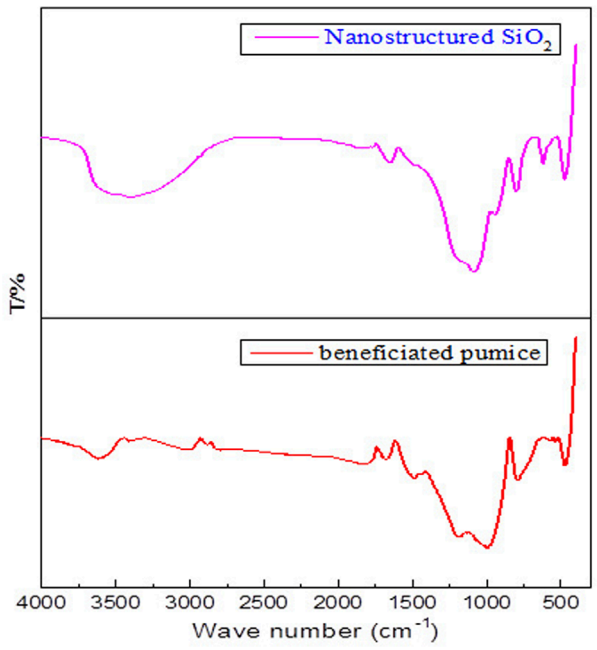

FIGURE 6
Highlights the FTIR spectra of beneficiated pumice and pumice-derived nanostructured SiO_2.

silanol (Si–OH) groups (Ellerbrock et al., 2022), 1,650–1,630 cm^{-1} (H–O–H bending of molecular water), 1,050–1,000 cm^{-1} and 820–750 cm^{-1} (Si–O–Si asymmetric and symmetric stretching, respectively), and 550–450 cm^{-1} (Si–O bending). Additional bands at 1,500–1,350 cm^{-1} indicate C–O stretching, and peaks at 960–850 cm^{-1} correspond to Al–O–Si stretching in aluminosilicates, while the peak at 870 cm^{-1} (out-of-plane bending of carbonate ions) indicates the presence of carbonates. Peaks below 500 cm^{-1} correspond to Al–O and Fe–O metal-oxygen bonds, consistent with prior studies (Demir et al., 2019; Meftah et al., 2023).

The FTIR spectrum of the synthesized nanostructured SiO_2 reveals characteristic features of high-purity silica, closely matching the spectra of commercial high-performance silica (Günkaya and Banar, 2018; Hidayah, 2024).

Key peaks include O–H stretching vibrations at 3,650–3,250 cm^{-1}, attributed to surface hydroxyl groups and adsorbed moisture, and H–O–H bending vibrations at 1,650–1,630 cm^{-1}, corresponding to molecular water. These features are commonly observed in high-performance silica, which has a high surface area and exhibits hydrophilicity, resulting in greater moisture adsorption (Mourhly et al., 2019).

In addition, bands at 1,150–1,050 cm^{-1} and 850 cm^{-1}, corresponding to Si–O–Si asymmetric and symmetric stretching vibrations, respectively (Ellerbrock et al., 2022), confirm the presence of a well-organized silica network. The peak at 500–450 cm^{-1} is attributed to Si–O bending vibrations (Ellerbrock et al., 2022), which further indicate a well-structured silica matrix, typical of commercial-grade silica. The absence of peaks related to impurities (Johannesen et al., 1954) confirms that the synthesized SiO_2 is highly pure, achieved through a combination of beneficiation, alkaline leaching, and sol-gel synthesis, which effectively reduces impurities to undetectable levels.

In FTIR spectra, the loss on ignition (LOI) decreases from pumice to nanostructured SiO_2. The more prominent and intense O–H stretching (~3,400 cm^{-1}) and bending (~1,630 cm^{-1}) bands in nanostructured SiO_2 are attributed to its higher surface area and increased concentration of surface silanol (Si–OH) groups. During the synthesis process, the removal of impurities and structural reorganization exposes more hydroxyl groups on the silica surface, leading to stronger O–H signals despite the overall reduction in bound water and impurities (Ellerbrock et al., 2022).

The high concentration of surface hydroxyl groups, resulting from the material's increased surface area and amorphous nanostructure, enhances surface reactivity, making it highly suitable for applications such as rubber reinforcement, adsorption, and catalysis. These structural characteristics, combined with the spectral features, demonstrate that the synthesized Ethiopian

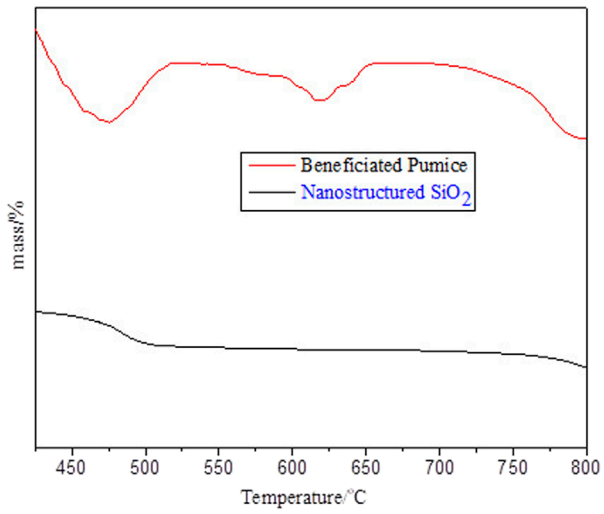

FIGURE 7
Depicts the TGA thermograms of beneficiated pumice and pumice-derived nanostructured SiO_2, showcasing thermal stability.

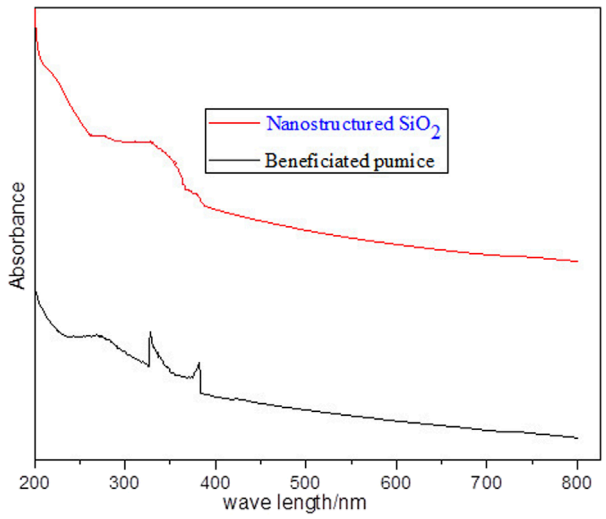

FIGURE 8
Presents the UV–Vis absorbance spectra of beneficiated pumice and pumice-derived nanostructured SiO_2.

pumice-derived SiO_2 exhibits properties comparable to commercial high-performance nanostructured silica, confirming its potential for advanced industrial applications (Raza, 2019).

3.4 Thermal stability analysis: TGA

The thermogravimetric analysis (TGA) of beneficiated pumice exhibited a step-wise weight loss pattern as shown in Figure 7, indicating the gradual decomposition of its components. The initial weight loss below 400°C was attributed to the evaporation of moisture and the release of physically bound water. A sharp decrease in weight between 400°C and 450°C was associated with the decomposition of organic matter and volatile compounds. The weight remained stable between 450°C and 475°C, suggesting that most organic materials had decomposed. A slight weight gain between 475°C and 525°C was likely caused by the oxidation of residual impurities, such as metal oxides. From 525°C to 600°C, the weight remained constant, indicating thermal stability in this range. Another weight gain between 625°C and 650°C may have resulted from further oxidation of inorganic components. The weight remained stable from 675°C to 750°C, reflecting the thermal stability of the material's inorganic matrix. A sharp weight loss occurred above 775°C, which was attributed to the decomposition or phase transformation of structural hydroxyl groups and high-temperature compounds like carbonates, releasing gases such as CO_2. This step-wise weight loss pattern demonstrated the complex thermal decomposition and compositional diversity of beneficiated pumice, consistent with previous findings (Mourhly et al., 2015; Hidayah, 2024).

In contrast, the nanostructured SiO_2 exhibited a more pronounced weight loss below 100°C, primarily due to the evaporation of residual moisture. The weight loss continued up to approximately 500°C, after which the material became thermally stable, with minimal or no further loss as shown in Figure 7, indicating the robust thermal stability of silica. This stability above 500°C is characteristic of the silica network, which is inherently stable due to its high-temperature resistance. Thus, the enhanced thermal stability of nanostructured SiO_2 was validated by its behavior above 500°C, where it maintained its mass, unlike the beneficiated pumice, which continued to show weight loss even at higher temperatures (Mourhly et al., 2019). Alkaline leaching and calcination effectively removed organic and inorganic impurities, resulting in minimal mass loss beyond 500°C. This indicated the high purity of the synthesized SiO_2, consistent with previous studies (Li et al., 2012), which demonstrated that reduced impurity content and increased silica concentration contribute to improved thermal stability.

This enhanced thermal stability is linked to the effective removal of impurities and the formation of high-purity silica, making it well-suited for high-temperature applications such as rubber reinforcement, thermal insulation, and catalysis, as supported by previous research (Zhang et al., 2024).

3.5 UV–vis analysis of optical properties

The ultraviolet–visible (UV–Vis) spectra presented in Figure 8 highlight distinct differences between beneficiated pumice and pumice-derived nanostructured silica. The beneficiated pumice shows multiple broad peaks, indicating impurities such as metal oxides and organic residues, consistent with Hidayah (2024). In contrast, the nanostructured silica exhibits a characteristic broad peak at approximately 297 nm, attributed to intrinsic electronic transitions in the silica network, particularly the UV absorption of oxygen-silicon (Si–O) bonds (Luthfiah et al., 2021). This peak reflects the silica's UV absorbance properties and indicates high optical purity.

The UV–Vis results show minimal light absorption in the visible region, confirming the high optical transparency and purity, as

TABLE 2 BET summary of beneficiated pumice and pumice nano SiO_2.

Sample name	Surface area (m^2/g)	Pore volume (cm^3/g)	Pore size (nm)
Beneficiated pumice	335.167	6.301×10^{-14}	0.9237 nm
Pumice nano SiO_2	571.477	8.663×10^{-14}	0.9237 nm

reported by Meftah et al. (2023) and Thahab Al-Abboodi et al. (2020). The purification and nanoscale processing of the beneficiated pumice significantly enhance its optical properties, aligning with previous studies (Bachir et al., 2023), which show that the nanosilica derived from natural materials exhibits well-defined absorbance peaks due to reduced impurities and intrinsic optical characteristics. This study demonstrates the optical refinement achieved through the synthesis of nanosilica from pumice.

3.6 Surface texture and pore structure analysis (BET method)

The BET analysis (Table 2; Figures 9A, B) reveals a significant increase in the surface area and pore volume following the transformation of Ethiopian pumice into nanostructured SiO_2.

The surface area increased from 335.167 m^2/g (pumice) to 571.477 m^2/g (nanostructured SiO_2), exceeding the values reported in previous studies, which were found to be 25 m^2/g to 30 m^2/g (Kalapathy et al., 2002), 16–37 m^2/g (Sulaiman et al., 2022), 60–120 m^2/g (Khanday, 2018), 100–200 m^2/g (Sharafudeen et al., 2017), 358 m^2/g (Sarikaya et al., 2017), and 422 m^2/g (Mourhly et al., 2019). However, it is slightly lower than the 670.8 m^2/g reported in one study (Raza et al., 2018). Additionally, the pore volume expanded from 6.301×10^{-14} cm^3/g to 8.663×10^{-14} cm^3/g. These improvements are particularly beneficial for applications such as rubber reinforcement, adsorption, filtration, and catalysis. The optimized synthesis of nanostructured SiO_2 in this study resulted in a well-defined morphology with a high surface area (571.48 m^2/g) and controlled pore characteristics (86.63 nm). The synthesized silica exhibits properties suitable for rubber-grade fillers, demonstrating superior reinforcement capabilities compared to commercial silica fillers. Its BET surface area exceeds that of quartz-based and most biogenic silica sources, thereby enhancing its performance as both a filler and a reinforcing agent. This structural optimization improves adsorption efficiency by increasing the available surface area for molecular interactions and enhances catalytic performance by facilitating greater access of reactants to active sites. Utilizing abundant Ethiopian pumice offers a sustainable, cost-effective alternative to energy-intensive synthetic and mineral-derived silica and promotes the development of environmentally friendly materials.

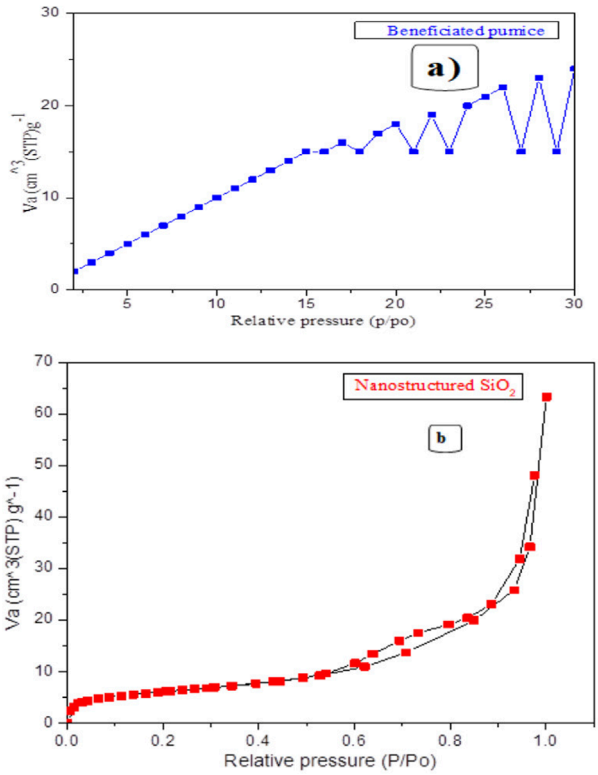

FIGURE 9
Illustrates the BET isotherms of beneficiated Ethiopian pumice **(A)** and pumice-derived nanostructured SiO_2 **(B)**.

3.7 Particle size analysis by DLS

The DLS analysis (Figure 10) confirms the successful synthesis of uniform nanostructured SiO_2 with a narrow particle size distribution ranging from 10 nm to 100 nm. This contrasts sharply with the broader distribution observed in beneficiated pumice, which ranges from 600 nm to 10,000 nm. As highlighted in previous studies (Amer, 2020), such uniformity improves material consistency and performance, making it highly suitable for applications such as rubber reinforcement, catalysis, and adsorption. The particle size distribution of beneficiated pumice (Figure 10A) reveals a heterogeneous, polydisperse distribution with peaks between 600 nm and 10,000 nm.

This broad distribution is attributed to the mixed mineral and organic components present in untreated pumice, as described in a previous study (Ravindra, 2021). In contrast, the nanostructured SiO_2 (Figure 10B) shows a single dominant peak within the 10–100 nm range, confirming the synthesis of monodisperse SiO_2 with significantly reduced polydispersity, consistent with the findings of another study (Luthfiah et al., 2021).

This narrower distribution validates the successful transformation of Ethiopian pumice into high-performance nanostructured SiO_2, making it ideal for advanced applications such as rubber reinforcement, adsorption, and catalysis. The particle size distribution of nanostructured SiO_2 in the 10–100 nm range aligns with previous studies (Demir et al., 2019), indicating the production

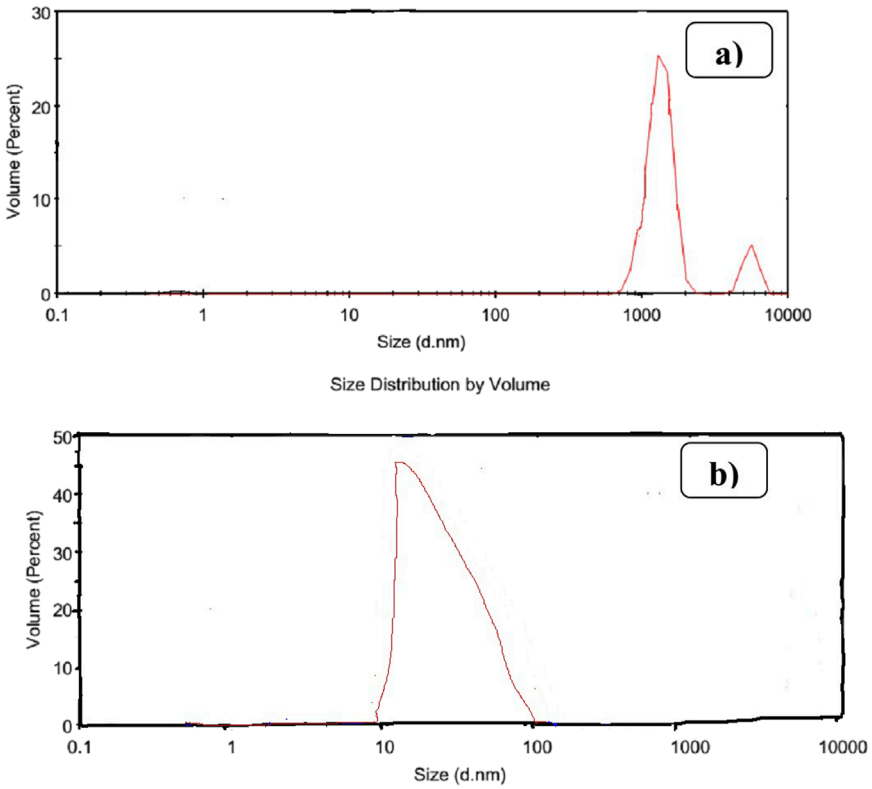

FIGURE 10
Shows the DLS analysis for particle size distribution of beneficiated pumice **(A)** and pumice-derived SiO_2 **(B)**.

of a high-performance SiO_2 filler with minimal agglomeration, which is critical for reinforcing rubber.

The correlogram for beneficiated pumice (Figure 11A) shows a gradual decay in the correlation, indicating larger particles and high polydispersity, consistent with raw mineral samples reported by Aziz (2014).

In contrast, the correlogram for nanostructured SiO_2 (Figure 11B) displays a sharp initial drop followed by exponential decay, confirming a more uniform particle size distribution. The gradual decrease to 0 suggests some residual aggregation, a common challenge in nanoparticle synthesis. These results demonstrate the successful conversion of Ethiopian pumice into nanostructured SiO_2 with reduced polydispersity.

Further improvements, such as surface functionalization or advanced dispersion techniques (Bachir et al., 2023), could enhance its performance, particularly for applications like rubber reinforcement.

3.8 Morphology and elemental composition analysis by SEM-EDAX

The SEM images (Figures 12, 13) illustrate the morphological transformation from beneficiated pumice to synthesized nanostructured SiO_2. Beneficiated pumice exhibited a heterogeneous morphology, while the nanostructured SiO_2 displayed uniform, spherical particles with minimal agglomeration, attributed to controlled nucleation and growth during the sol–gel synthesis process. The reduced agglomeration enhances the material's suitability for advanced applications such as rubber reinforcement and coatings.

The study successfully utilized 9.695 µm pumice particles to produce nanostructured SiO_2 with an average particle size of 35.83 nm, as shown in Figure 12. SEM-EDAX analysis (Figure 12; Table 3) of the beneficiated pumice revealed a composition of 47.1% oxygen, 40.59% silicon, 9.53% aluminum, and trace amounts of sodium, calcium, iron, and magnesium.

The EDAX spectra identified characteristic peaks at ~1.65 keV (Si Kα), ~1.5 keV (Al Kα), and ~6.5 keV (Fe Kα), reflecting the heterogeneous composition and presence of impurities (Mourhly et al., 2015). In contrast, the SEM-EDAX analysis of the synthesized nanostructured SiO_2 (Figure 13; Table 4) confirmed its high purity, with 98.52% of its composition consisting of silicon and oxygen, and only 1.48% of metal oxides remaining, an impurity level negligible for high-performance applications.

The uniform nanoscale morphology and high purity of the synthesized SiO_2 highlight its potential for use in optics, electronics, rubber fillers, and catalysis. The successful synthesis of 35.83 nm nanostructured SiO_2 from Ethiopian pumice demonstrates the efficacy of the sol–gel method, aligning with findings from previous studies (Meftah et al., 2023; Bachir et al., 2023).

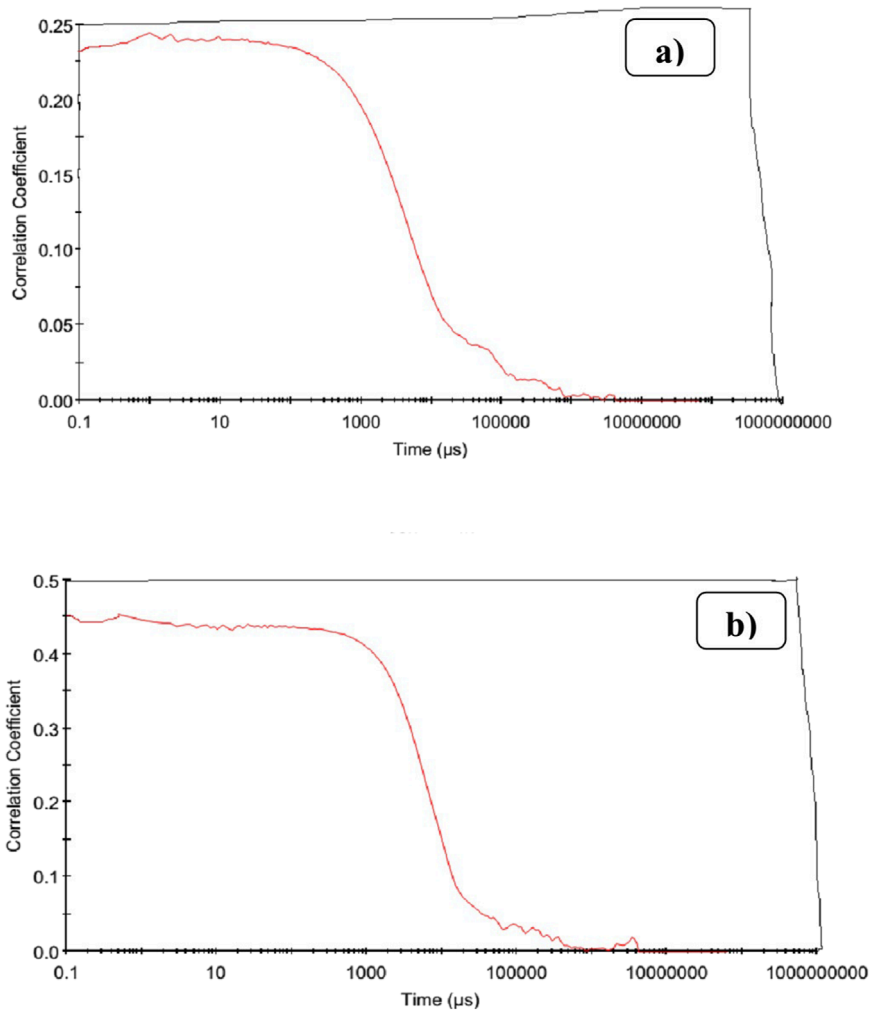

FIGURE 11
Presents the correlograms of beneficiated pumice **(A)** and pumice-derived nanostructured SiO_2 **(B)**.

3.9 Mass balance and yield of 0D nanostructured SiO_2

The synthesis of nanostructured SiO_2 from Ethiopian pumice involves a multi-step process, including alkaline extraction, precipitation, washing, acid purification, drying, and calcination.

Using 30 g of Ethiopian pumice containing 64.82% SiO_2, the theoretical silica content is calculated as

$$\text{Theoretical } SiO_2 \text{ content (g)} = 30 \times \frac{64.82}{100} = 19.45 \text{ g}.$$

During alkaline leaching, pumice reacts with NaOH to form sodium silicate, with an extraction efficiency of 90%, yielding approximately:

$$SiO_2 \text{ in solution (g)} = 19.45 \times 0.90 = 17.51 \text{ g}.$$

Subsequent precipitation with H_2SO_4, with an efficiency of 85%, results in

$$\text{Precipitated } SiO_2 \text{ (g)} = 17.51 \text{ g} \times 0.85 = 14.88 \text{ g}.$$

Acid purification with HCl removes residual impurities with 95% efficiency, yielding

$$\text{Purified } SiO_2 \text{ (g)} = 14.88 \times 0.95 = 14.14 \text{ g}.$$

Drying and calcination at 600°C remove adsorbed water and residual organics, resulting in a final yield of

$$\text{Final } SiO_2 \text{ yield (g)} = 14.14 \times 0.95 = 13.43 \text{ g}.$$

The overall yield is calculated using the following equation:

$$\text{Yield (\%)} = \frac{13.43 \text{ g}}{19.45} \times 100 = 69.07\%.$$

Additionally, the mass balance is expressed as

Mass balance (%) = Total mass of products and by-products/Initial mass of raw pumice × 100.

Sodium sulfate (Na_2SO_4), a key by-product, is formed in this reaction. Using molar ratios, its mass is calculated as:

$$Na_2SO_4 \text{ (g)} = 14.88 \text{ g precipitated} \frac{SiO_2}{60.08 \text{ g}} \frac{SiO_2}{\text{mole}} \times 142.04 \text{ g } Na_2SO/\text{mole} = 35.20 \text{ g}.$$

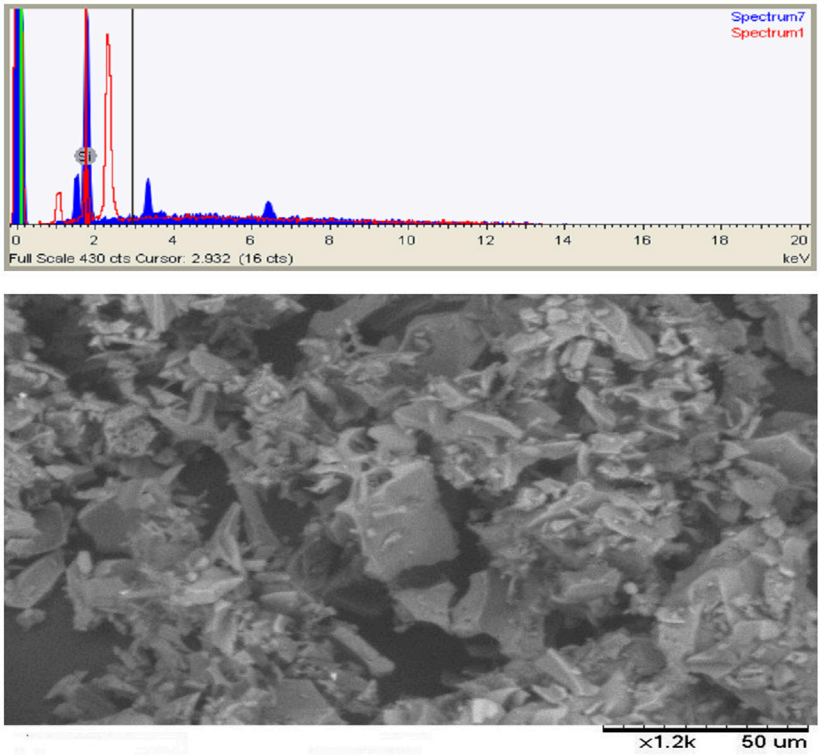

FIGURE 12
Images show the SEMEDAX analyses of beneficiated pumice; illustrating its morphology and elemental composition.

The total expected mass of products and by-products is

$$\text{Total mass of product \& by} - \text{product (g)} = 13.43\ \text{g} + 35.20\ \text{g} = 48.63\ \text{g}$$

The mass balance is calculated as

$$\text{Mass balance (\%)} = 48.63\ \text{g}/30\ \text{g} \times 100 = 162.10\%$$

The mass balance exceeds 100% due to the incorporation of sodium and sulfur during synthesis, which were not present in the original pumice. Additionally, the removal of impurities and evaporation of water during drying and calcination result in an apparent increase in total mass compared to the initial raw material. This outcome aligns with typical chemical processes where reaction by-products contribute to the overall mass. The high final yield (69.07%) demonstrates an efficient synthesis process, and the mass balance value reflects realistic reaction outcomes reported in similar silica extraction studies (Melis et al., 2022). The method yields high-purity silica (98.52%), making it suitable for industrial applications. Moreover, the process is cost-effective, scalable, and supports sustainable material development by utilizing natural Ethiopian pumice.

3.10 0D nanostructured SiO_2

Zero-dimensional (0D) nanostructured SiO_2 nanoparticles are characterized by their nanoscale size and isotropic structure, typically forming spherical morphologies. The classification as 0D is based on their particle size and morphology, with dimensions confined to the nanoscale (1–100 nm). In this study, the synthesized SiO_2 particles have an average size of 35.83 nm, as confirmed by scanning electron microscopy (SEM), and a particle size distribution of 10–100 nm, as confirmed by dynamic light scattering (DLS). These particles are spherical and lack extended directional growth, which is typical of 0D nanomaterials (Paras et al., 2023).

Unlike one-dimensional (1D) (nanorod) or two-dimensional (2D) (nanosheet) materials, which have extended structures, 0D materials are discrete, with no significant length, width, or height beyond the nanoscale. The uniform size distribution and spherical shape further support this classification.

The amorphous phase, with its high surface area, reactive silanol groups, and ease of surface functionalization, is preferred for applications in catalysis, reinforcement fillers, and adsorption (Zhuravlev, 2000). Thus, the prepared nanostructured SiO_2 is amorphous and 0D, with properties suitable for advanced industrial applications.

3.11 Potential of nanostructured SiO_2 for high-performance applications

In our study, we have not directly tested the material's performance in specific applications such as rubber reinforcement or catalysis. However, the synthesized nanostructured SiO_2 from Ethiopian pumice exhibits key physicochemical properties that are

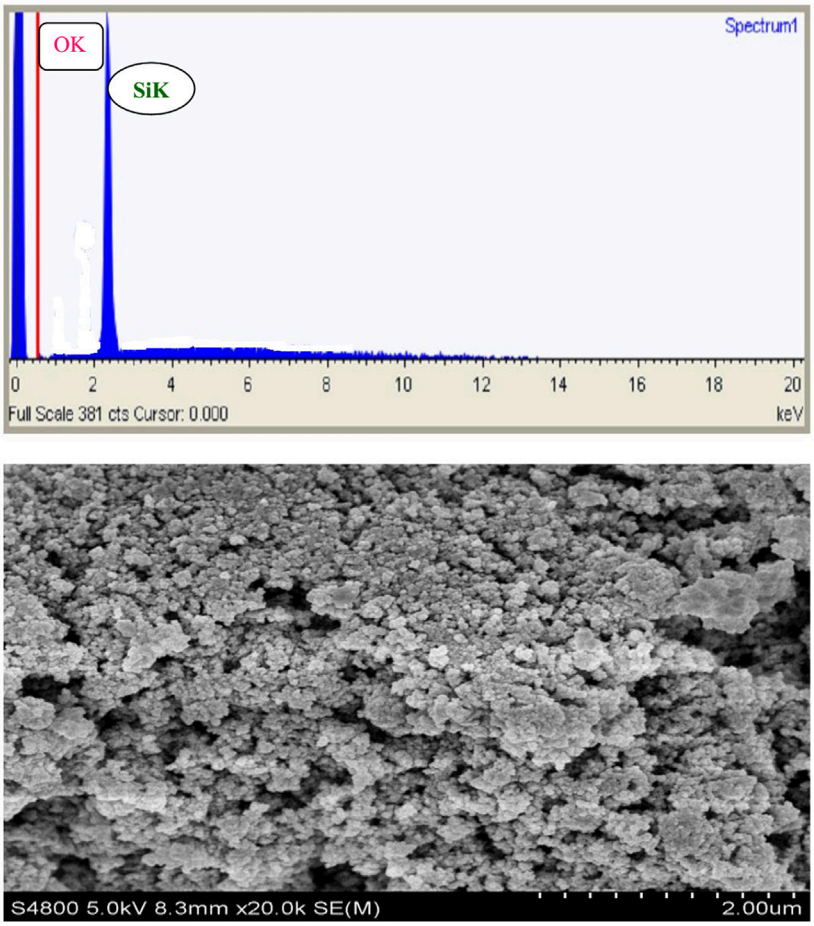

FIGURE 13
Images show the SEM-EDAX analysis of beneficiated pumice and pumice-derived nanostructured SiO_2, respectively, illustrating their morphology and elemental composition.

TABLE 3 Summary of EDAX elemental analysis of Ethiopian beneficiated pumice.

Element	Weight %
OK	47.1
NaK	1.07
AlK	9.53
Si	40.59
CaK	1.33
FeK	2.16
MgK	0.36

TABLE 4 Summary of EDAX elemental analysis of pumice-derived nano SiO_2.

Element	Weight %
Oxygen	51.31
Silicon	47.21
Metal oxide impurities	1.48
Total amount	100%

typically associated with high-performance silica materials. Its high purity (98.52%), significant yield (69.07%), and uniform nanoscale particle size distribution (average primary size of 35.83 nm, with a hydrodynamic diameter range of 10–100 nm) ensure consistent material quality. The high specific surface area (571.48 m^2/g) and mesoporosity (pore volume of 0.74 cm^3/g, average pore size of 86.63 nm) provide abundant active sites for surface interactions, enhancing its potential for demanding applications. Additionally, its thermal stability up to greater than 900°C and minimal weight loss beyond 500°C indicate resilience in high-temperature environments, while its optical purity reflects low impurity content.

These properties align with those reported in the literature for high-performance silica materials. For example, in rubber composites, a high surface area improves interfacial bonding with the polymer matrix, enhancing mechanical properties like tensile strength and elastic modulus. The nanoscale particle size ensures better dispersion, reducing filler aggregation and facilitating efficient stress transfer, which are features comparable to commercial fillers such as Ultrasil VN3. These results align with the findings reported by Brinke (2002). Similarly, in catalysis, the high surface area and mesoporosity provide abundant active sites, facilitating reactions such as hydrogenation and acid-catalyzed processes.

Additionally, its thermal stability enables operation at elevated temperatures, as reported by Song et al (2020). The material's small particle size, large surface area, and pore volume also suggest its suitability for drug delivery, enabling efficient therapeutic agent loading, cellular uptake, and controlled release. Saha (2020) showed that silica materials with similar properties are effective for controlled and targeted drug delivery.

While further application-specific performance tests are needed to fully validate these claims, the combination of high purity, nanoscale uniformity, large surface area, mesoporosity, and thermal stability indicates that the synthesized nanostructured SiO_2 possesses essential properties required for high-performance applications across various industries.

3.12 Comparison of 0D nanostructured SiO_2 from various sources

This section compares the zero-dimensional (0D) nanostructured SiO_2 synthesized from Ethiopian pumice with SiO_2 produced from other sources, focusing on particle size, surface area, morphology, and application potential in rubber composites. The comparison of nanostructured silica from various sources proves the novelty and significance of our synthesized silica derived from Ethiopian pumice. Our material, synthesized through purification, wet-process alkaline leaching, and sol–gel precipitation, shows a high surface area of 571.48 m^2/g, a pore size of 86.63 nm, and a purity of 98.52%, making it highly suitable for rubber reinforcement filler, catalysis, adsorption, and optoelectronics applications.

In contrast, silica from rice husk biomass (combustion and acid treatment) shows a lower surface area of 25–30 m^2/g with high purity but lacks specified pore size and applications (Kalapathy et al., 2002). Silica sand produced via the sol–gel method has a surface area of 16–37 m^2/g with high purity and is mainly used as a plant stimulant (Sulaiman et al., 2022). Quartz sand prepared directly used in hybrid silicon solar cells but lacks specific quantitative data (Al-Akhras et al., 2018). Bamboo leaf ash treated by combustion and acid washing has a surface area of 80–90 m^2/g with high purity for adsorption and catalysis (Yao et al., 2020).

Diatomaceous earth produced through acid digestion shows a surface area of 60–120 m^2/g for water purification and catalysis (Khanday, 2018). Fly ash treated with acid and the sol–gel process exhibits a surface area of 45–60 m^2/g for environmental remediation and composites (Garg, 2021). Morocco pumice rock processed similarly to our method has a lower surface area of 422 m^2/g, a pore size of 5.5 nm, and 94.44% purity for catalyst support (Mourhly et al., 2019). Olivine produced through leaching achieves a higher surface area of 670.8 m^2/g with smaller pores (5.59 nm) and lower purity (86.8%) (Raza et al., 2018). Desert sand produced using alkali fusion shows a 100–200 m^2/g surface area with 10–30 nm pores for water treatment (Sharafudeen et al., 2017). Perlite produced from wet processing has particle sizes of 0.3–1 μm with 98% purity for insulation materials (Srivastava et al., 2013). Turkish pumice produced via alkaline treatment yields a 358 m^2/g surface area with a mesoporous structure for catalytic applications (Sarikaya et al., 2017).

Compared to all these, our silica's exceptionally high surface area, tailored pore size, and high purity highlight its novelty, offering a sustainable and cost-effective solution with superior performance for industrial applications, particularly in rubber reinforcement.

3.13 Comparison of 0D SiO_2 with commercial SiO_2

The nanostructured 0D SiO_2 synthesized in this study exhibits a significantly higher BET surface area (571.48 m^2/g) than high-performance commercial silica such as Ultrasil VN3 (170–220 m^2/g), with a comparable pore volume (0.74 cm^3/g vs. 0.75 cm^3/g) and similar particle size distribution (10–100 nm) (HB Chemical, 2022). Similarly, its average particle size (~38 nm) falls within the range of commercial silica (~25–50 nm), and both materials share an aggregated, near-spherical, porous morphology. The higher surface area of the synthesized silica enhances polymer–filler interactions, contributing to its comparable reinforcement efficiency in NR/SBR rubber composites, aligning well with established commercial standards (Brinke, 2002). This comparison highlights the potential of our pumice-derived silica as a high-performance reinforcement filler in rubber applications (Evonik, 2023).

4 Conclusion

This study successfully transformed Ethiopian pumice into high-purity nanostructured silica through beneficiation, alkaline leaching, and sol–gel precipitation. The synthesized silica exhibited enhanced structural, thermal, and optical properties, including a high BET surface area (571.48 m^2/g), an average pore size (86.63 nm), and a uniform nanoscale particle size distribution (10–100 nm). These characteristics highlight its suitability for high-performance industrial applications such as rubber reinforcement, catalysis, adsorption, and optoelectronics. Compared to other silica sources, our material offers superior surface area, tailored pore size, and high purity (98.52%), making it a sustainable and cost-effective solution for advanced material applications, particularly in the rubber industry. The optimized process achieved a yield of 69.07%, within the upper range reported in the literature, confirming its efficiency and potential scalability.

This study introduces Ethiopian pumice as an underutilized volcanic rock source, presenting a sustainable alternative to synthetic and high-energy mineral-based silica production. The high-performance properties of the synthesized silica, including enhanced polymer-filler interactions and comparable reinforcement efficiency to commercial silica such as Ultrasil VN3

(HB Chemical, 2022), highlight its potential for reinforcing rubber composites (Evonik, 2023).

Future research should prioritize scaling up the synthesis of pumice-derived 0D SiO_2 nanoparticles, optimizing reaction conditions, energy efficiency, and cost-effectiveness while maintaining high material quality (Kumar et al., 2024; Choudhury, 2023). Collaboration with industry partners is essential to ensure sustainable and scalable production. Pilot trials in tire formulations should evaluate mechanical performance, thermal stability, and wear resistance, positioning pumice-derived silica as a sustainable, high-performance alternative to conventional silica. Our green synthesis method, using affordable reagents (NaOH, H_2SO_4, and HCl) and simple techniques, operates under mild conditions, minimizes waste, and avoids toxic solvents, making it environmentally friendly and scalable. This approach adds value to Ethiopian pumice, enabling its use in industrial applications like rubber reinforcement, coatings, and composites. Its future application in Ethiopia's tire industry, particularly at the Horizon Addis Tire factory, could significantly contribute to import substitution and the sustainable utilization of local resources, promoting industrial growth and advancing sustainable materials research.

Data availability statement

The raw data supporting the conclusions of this article will be made available by the authors, without undue reservation.

Author contributions

AM: conceptualization, writing – review and editing, data curation, formal analysis, investigation, methodology, visualization, and writing – original draft. GE: conceptualization, methodology, project administration, resources, supervision, and writing – review and editing. FS: conceptualization, methodology, project administration, resources, software, supervision, and writing – review and editing.

Funding

The author(s) declare that no financial support was received for the research and/or publication of this article.

Acknowledgments

Agraw Mulat would like to acknowledge ASTU for providing the PhD opportunity and laboratory access during his studies. He also acknowledges the support of Assosa University, his academic affiliation, for providing the resources and environment necessary to complete this research. He is deeply grateful to his main advisor, Gemechu Deressa (Associate Professor), and his co-advisor, Fedilu Kedir (Associate Professor), for their expert guidance, insightful feedback, and unwavering support throughout this journey. Lastly, he appreciates his family's endless love, patience, and encouragement, which have been a constant source of strength.

Conflict of interest

The authors declare that the research was conducted in the absence of any commercial or financial relationships that could be construed as a potential conflict of interest.

Generative AI statement

The author(s) declare that no Generative AI was used in the creation of this manuscript.

Publisher's note

Supplementary material

The Supplementary Material for this article can be found online at: https://www.frontiersin.org/articles/10.3389/fmats.2025.1566490/full#supplementary-material

References

Adam, F., Chew, T. S., and Andas, J. (2011). A simple template-free sol-gel synthesis of spherical nanosilica from agricultural biomass. *J. Sol-Gel Sci. Technol.* 59 (3), 580–583. doi:10.1007/s10971-011-2531-7

Al-Akhras, M. A., Arunmetha, S., Vinoth, M., Srither, S. R., Karthik, A., Sridharpanday, M., et al. (2018). Study on production of silicon nanoparticles from quartz sand for hybrid solar cell applications. *J. Electron. Mater.* 47 (1), 493–499. doi:10.1007/s11664-017-5794-0

Alves, R. H., Reis, T. V. d. S., Rovani, S., and Fungaro, D. A. (2017). Green synthesis and characterization of biosilica produced from sugarcane waste ash. *Hindawi J. Chem.* 2017, 1–9. doi:10.1155/2017/6129035

Amer, A. A., El-Fadaly, E., and Abazeed, I. H. (2020). Synthesis and characterization of low cost nanosilica from sodium silicate solution and their applications in ceramic engobes. *elsevier* 59, 31–43. doi:10.1016/j.bsecv.2019.06.004

Aziz (2014). Synthesis of silica nanoparticles from silica sand via sol-gel method. *J. Mater. Res. Technol.* 3 (4), 363–367. doi:10.1016/j.jmrt.2014.10.001

Bachir, B. B. S., Hemmami, H., Hocine, B. M. E., Soumeia, Z., Sharifi-Rad, M., Awuchi, C. G., et al. (2023). Methods for the preparation of silica and its nanoparticles from different natural sources. *Biol. Trace Elem. Res.* 201 (12), 5871–5883. doi:10.1007/s12011-023-03628-w

Bageru, A. B., and Srivastava, V. C. (2018). Efficient teff-straw based biocomposites with chitosan and alginate for pyridine removal. *Int. J. Environ. Sci. Technol.* 16 (10), 5757–5766. doi:10.1007/s13762-018-1957-7

Beneditt-Jimenez, Ulloa-Castillo, N. A., Iturbe-Ek, J., Martínez-Romero, O., Elías-Zúñiga, A., and Sustaita, A. O. (2022). A hybrid superhydrophobic/hydrophilic surface based on SiO_2 nanoparticles over a clay substrate for enhanced dew yield potential. *Appl. Sci.* 12 (3), 1526. doi:10.3390/app12031526

Brinke, T. (2002). *Silica reinforced tyre rubbers*. Ph.D. thesis (Enschede, Netherlands: University of Twente).

Brinker, C. J., and Scherer, G. W. (1990). *Sol-gel science: the physics and chemistry of sol-gel processing*. San Diego: Academic Press.

Choudhury, A. (2023). Green Nanotechnology: an innovative pathway for sustainability. *Indian J. Res.* 12 (1), 1–3. doi:10.36106/paripex

Crangle, R. D. (2019). Pumice and pumicite. *Min. Eng.* 70 (7), 78–79.

Demir, F., Demir, E. M., Sharma, A., Dal, M., El-Mallawany, R., and Kaçal, M. (2019). Investigation ofthe gamma ray shielding parameters of (100-x)[0.5Li2O–0.1B2O3–0.4P2O5]-xTeO2 glasses using Geant4 and FLUKA codes. *J. Non-Crystalline Solids* 521, 119489. doi:10.1016/j.jnoncrysol.2019.119489

Dizgeet, N. (2022). A review of hybrid process development based on electrocoagulation for thetreatment of textile and dyeing industry wastewater. *Int. J. Environ. Res.* (19) 3, 1105–1126. doi:10.1007/s13762-021-03441-0

Ellerbrock, R., Stein, M., and Schaller, J. (2022). Comparing amorphous silica, short-range-ordered silicates and silicic acid species by FTIR. *Sci. Rep.* 2, 11708. doi:10.1038/s41598-022-15882-4

Emrie, D. B. (2024). Sol–gel synthesis of nanostructured mesoporous silica powder and thin films. *Hindawi J. Nanomater.* 2024, 1–16. doi:10.1155/2024/6109770

Evonik (2023). Solutions for the tire and rubber industry. Available online at: https://products.evonik.com/assets/49/76/IB306_Solutions_for_the_tire_and_rubber_industry_EN_EN_244976.pdf (Accessed February 24, 2025).

Garg, A. (2021). Synthesis of nanosilica from fly ash for applications in water treatment and environmental remediation. *Environ. Sci. Pollut. Res.* 28 (2), 2450–2460. doi:10.1007/s11356-020-09759-x

Gebretatios, A. W., and Raghavan, A. S. (2021). Synthesis and characterization of nanostructured silica from teff straw (Eragrostis tef) using a sol-gel method. *Mater. Chem. Phys.* 267, 124678. doi:10.1016/j.matchemphys.2021.124678

Geda, A., and Shimeles, A. (2007). The structure and performance of Ethiopia's manufacturing sector: an overview. *J. Afr. Econ.* 16 (5), 761–822. doi:10.1093/jae/ejm015

Günkaya, Z., and Banar, M. (2018). Pumice as a raw material for high-value nanomaterials: a review. *J. Clean. Prod.* 172, 2536–2548. doi:10.1016/j.jclepro.2017.11.150

Hani, A., Meftah, N., Zeghoud, L., Sdiri, A., and Jawad, A. H. (2023). Statistical optimization and desirability function for producing nano silica from dune sand by sol–gel method towards methylene blue dye removal. *J. Inorg. Organomet. Polym. Mater.* 33 (7), 1882–1897. doi:10.1007/s10904-023-02612-0

HB Chemical (2022). Ultrasil VN3 - technical data sheet. Available online at: https://www.hbchemical.com/wp-content/uploads/2022/09/ULTRASIL-VN-3-EN.pdf (Accessed February 24, 2025).

Hidayah, R., Kurniawati, D., and Alizar, A. (2024). Characterization of silica nanoparticles from pumice as an aerogel adsorbent, 7(1), p. 01. doi:10.24114/ijcst.v7i1.56435

Imoisili, P. E., and Jen, T.-C. (2022). Microwave-assisted sol–gel template-free synthesis and characterization of silica nanoparticles obtained from South African coal fly ash. *Nanotechnol. Rev.* 11 (1), 3042–3052. doi:10.1515/ntrev-2022-0476

Imoisili, P. E., Ukoba, K. O., and Jen, T. C. (2020). Synthesis and characterization of amorphous mesoporous silica from palm kernel shell ash. *Elsevier Ceram.* 59, 159–164. doi:10.1016/j.bsecv.2019.09.006

Jembere, A. L. (2017). Studies on the synthesis of silica powder from rice husk ash as reinforcement filler in rubber tire tread part: replacement of commercial precipitated silica. *Int. J. Mater. Sci. Appl.* 6 (1), 37. doi:10.11648/j.ijmsa.20170601.16

Johannesen, R. B., Gordon, C., Stewart, J., and Gilchrist, R. (1954). Application of infrared spectroscopy to the determination of impurities in titanium tetrachloride. *J. Re se arc h Natl. Bureau Stand.* 53 (No. 4), 197–204. doi:10.6028/jres.053.024

Kalapathy, U., Proctor, A., and Shultz, J. (2002). An improved method for production of silica from rice hull ash. *Bioresour. Technol.* 85 (3), 285–289. doi:10.1016/s0960-8524(02)00116-5

Karande, V. S., Jadhav, S. A., Garud, H. B., Kalantre, V. A., Burungale, S. H., and Patil, P. S. (2021). Green and sustainable synthesis of silica nanoparticles. *Nanotechnol. Environ. Eng.* 6 (29), 29–15. doi:10.1007/s41204-021-00124-1

Kebede, T. G. (2020). Characterization and utilization of Ethiopian pumice as a sustainable raw material for industrial applications. *J. Appl. Sci.* 41 (8), 670–681. doi:10.3923/jas.2020.670.681

Khanday, F. A. (2018). Synthesis of silica nanoparticles from diatomaceous earth and their application in environmental remediation. *J. Environ. Chem. Eng.* 6 (1), 112–121. doi:10.1016/j.jece.2017.11.032

Khattak, S., Gul, S., Sultana, S., Noor-ul-Amin, (2023). Synthesis and characterization of nano-silica from locally available laterite clay. *Clay Miner.* 58, 408–414. doi:10.1180/clm.2023.36

Kumar, A., Tyagi, P. K., Tyagi, S., and Ghorbanpour, M. (2024). Integrating green nanotechnology with sustainable development goals: a pathway to sustainable innovation. *Discover* 5 (364), 364–413. doi:10.1007/s43621-024-00610-x

Kumar, R. (2019). The industrial uses of pumice: from filtration to construction. *J. Industrial Mater.* 48 (6), 1015–1024.

Kumar, R., and Prakash, K. H. (2019). A comprehensive review of sustainable synthesis strategies for silica nanoparticles. *Green Chem.* 21 (24), 6606–6627. doi:10.1039/C9GC02886C

Kumar, S. (2017). Synthesis and characterization of silica nanoparticles from wheat husk and their application as a reinforcing agent in composites. *J. Mater. Sci. Mater. Electron.* 28 (18), 13820–13826. doi:10.1007/s10854-017-7227-5

Laskowski, J., Laskowska, M., Vila, N., Schabikowski, M., and Walcarius, A. (2019). Mesoporous silica-based materials for electronics-oriented applications. *Molecules* 24 (13), 2395. doi:10.3390/molecules24132395

Lee, J. (2014). Solvothermal synthesis of monodisperse silica nanoparticles and their application as a template for hollow nanostructures. *J. Colloid Interface Sci.* 432, 285–290. doi:10.1016/j.jcis.2014.06.034

Li, Z., Barnes, J. C., Bosoy, A., Stoddart, J. F., and Zink, J. I. (2012). Mesoporous silica nanoparticles in biomedical applications. *Chem. Soc. Rev.* 41 (7), 2590–2605. doi:10.1039/c1cs15246g

Luthfiah, A., Deawati, Y., Firdaus, M. L., Rahayu, I., and Eddy, D. R. (2021). Silica from natural sources: a review on the extraction and potential application as a supporting photocatalytic material for antibacterial activity. *Sci. Technol. Indonesia* 6, 144–155. doi:10.26554/sti.2021.6.3.144-155

Manurung, P., Simanjuntak, R. M., and Ginting, E. (2022). Synthesis and characterisation of nano-silica based on pumice using NaOH. *J. Phys. Sci.* 33 (1), 17–28. doi:10.21315/jps2021.33.1.2

Meftah, N., Hani, A., and Merdas, A. (2023). Extraction and physicochemical characterization of highly-pure amorphous silica nanoparticles from locally available dunes sand. *Chem. Afr.* 6, 3039–3048. doi:10.1007/s42250-023-00688-2

Melis, R., Kumar, P., and Silva, D.(2022). Efficient synthesis and ass balance in silica extraction processes. *J. Mat. Sci.* 58(4), 123–135. doi:10.1016/j.jmat.2022.03.015

Mohammed, A., Ahmed, Y. A., Ren, S., and Xu, C. C. (2021). Advances in recovery and utilization of carbon dioxide: a brief review. *J. Environ. Chem. Eng.* 9 (5), 105644. doi:10.1016/j.jece.2021.105644

Mourhly, A., Khachani, M., El Hamidi, A., Kacimi, M., Halim, M., and Arsalane, S. (2015). The synthesis and characterization of low-cost mesoporous silica from local pumice rock. *Nanomater. Nanotechnol.* 5 (35), 1–8. doi:10.5772/62033

Mourhly, A., Jhilal, F., El Hamidi, A., Halim, M., and Arsalane, S. (2019). Highly efficient production of mesoporous nano-silica from unconventional resource: process optimization using a Central Composite Design. *Microchem. J.* 145, 139–145. doi:10.1016/j.microc.2018.10.030

Muhammud, A. M., and Gupta, N. K. (2022). Nanostructured SiO_2 material: synthesis advances and applications in rubber reinforcement. *RSC Adv.* 12 (18), 18524–18546. doi:10.1039/D2RA02747J

Mulugeta, M., and Tadesse, M. (2018). Exploring the industrial potential of Ethiopian pumice for nanostructured material synthesis. *J. Min. Mater. Eng.* 27 (3), 185–194. doi:10.11648/j.jmme.2018.03.06.11

Ogunbiyi (2019). Physico-chemical properties of pumice and its use in material synthesis. *J. Mater. Sci. Eng.* 60 (5), 312–321. doi:10.1016/j.jmse.2019.01.004

Paras, Yadav, K., Kumar, P., Teja, D. R., Chakraborty, S., Chakraborty, M., et al. (2023). A review on low-dimensional nanomaterials: nanofabrication, characterization and applications. *Nanomaterials* 13 (1), 160. doi:10.3390/nano13010160

Pereira, M. (2018). Environmental and economic impacts of silica extraction and processing. *Environ. Sci. and Technol.* 52 (14), 8032–8040. doi:10.1021/acs.est.8b01788

Rampe, M. J., Lombok, J. Z., Tiwow, V. A., Tengker, S. M. T., and Bua, J. (2023). Characterization of silica (SiO_2) based on beach sand from Sulawesi and Sumatra as silicon carbide (SiC) base material. *J. Chem. Technol. Metallurgy* 58 (3), 67–476. doi:10.59957/jctm.v58i3.75

Ravindra, R. (2021). Characterization of pumice for its industrial applications: silica content and properties. *Mater. Res. Innovations* 24 (12), 819–832. doi:10.1080/14328917.2020.1813583

Raza, N. (2019). Extraction and characterization of nano-silica from olive stones. *Springer Nat.* 12, 1–5. doi:10.1039/c8ra06257a

Raza, N., Raza, W., Madeddu, S., Agbe, H., Kumar, R., and Kim, K. H. (2018). Synthesis and characterization of amorphous precipitated silica from alkaline dissolution of olivine. *RSC* 8 (57), 32651–32658. doi:10.1039/c8ra06257a

Roco, M. C., and Bainbridge, W. S. (2002). Converging technologies for improving human performance: nanotechnology, biotechnology, information technology and cognitive science. *J. Nanoparticle Res.* 4 (1), 1–5. doi:10.1023/A:1016585030507

Rønning, M. G. T. (2004). Synthesis of nanostructured silica from olivine: a potential CO_2 mineral sequestration route. *Industrial and Eng. Chem. Res.* 43 (17), 5399–5406. doi:10.1021/ie049811v

Saha, R. S. V. P. and. S. S. (2020). Silica-based nanoparticles for drug delivery: synthesis, properties, and applications. *J. Nanosci. Nanotechnol.* 20 (1), 1–16. doi:10.1166/jnn.2020.17869

Santhosh, A., Velmurugan, V., Jacob, G., Jeong, S. K., Grace, A. N., and Bhatnagar, A. (2016). Role of nanomaterials in water treatment applications: a review. *Chem. Eng. J.* 306, 1116–1137. doi:10.1016/j.cej.2016.08.053

Sarikaya, M., Turan, M. D., Aydogmus, R., Yucel, A., Kizilkaya, N., and Depci, T. (2017). Extraction of meso-pores amorphous SiO_2 from van pumice. *Curr. Phys. Chem.* 7 (2), 1877–9468. doi:10.2174/1877946807666170808122455

Sharafudeen, J., Al-Hashim, J. M., Al-Harbi, M. O., Al-Ajwad, A. I., and Al-Waheed, A. A. (2017). Preparation and characterization of precipitated silica using sodium silicate prepared from Saudi Arabian desert sand. *Silicon* 9 (6), 917–922. doi:10.1007/s12633-016-9531-8

Shimomura, E. M. a. M. (2023). Synthesis and characterization of nanostructured silica powders using rice hull ash-based sodium silicate solution by precipitation and calcination. *Mater. Lett.* 17, 1–3. doi:10.1016/j.mlblux.2022.100175

Song, X., Liu, H., Zhang, W., Zhao, L., Li, Y., Wang, L., et al. (2020). CeO_2@SiO_2 core–shell nanostructure-supported CuO as high-temperature-tolerant catalysts for CO oxidation. *Langmuir* 36 (9), 2505–2513. doi:10.1021/acs.langmuir.0c00173

Srivastava, A., Yadav, M., Verma, N., Kumar, S., and Gupta, P., (2013). Pure silica extraction from perlite: its characterization and affecting factors. *International J. Innovative Res. Sci. Eng. Technol.* 2 (7), 2936–2942. doi:10.15680/IJIRSET.2013.0207008

Sulaiman, N. S., Hoang, C. V., Thoai, D. N., Cam, N. T. D., Phuong, T. T. T., Lieu, N. T., et al. (2022). Large-scale synthesis of nanosilica from silica sand for plant stimulant application in maize. *ACS Omega* 7 (9), 7810–7819. doi:10.1021/acsomega.2c05760

Thahab Al-Abboodi, S. M., Al-Shaibani, E. J. A., and Alrubai, E. (2020). Preparation and characterization of nano silica prepared by different precipitation methods. *IOP Conf. Ser. Mater. Sci. Eng.* 978 (1), 012031. doi:10.1088/1757-899X/978/1/012031

Thirumalai (2017). Silica-reinforced rubber composites: advances in tire performance and fuel efficiency. *Mater. Sci. Eng. R Rep.* 112, 33–47. doi:10.1155/2019/5891051

Wang, A. (2019). The role of silica as a reinforcing filler in rubber composites for tire applications. *J. Rubber Res.* 22 (2), 99–114. doi:10.1007/s42464-019-00007-0

Wang, Y. L. X. (2018). Flame synthesis of silica nanoparticles and their application in epoxy composites. *Mater. Chem. Phys.* 216, 1–7.

Yao, L., Jing, M., Xu, M., Han, D., Niu, Q., and Liu, R. (2020). Cytotoxicity of perfluorodecanoic acid on mouse primary nephrocytes through oxidative stress: combined analysis at cellular and molecular levels. *J. Hazard. Mater.* 393, 122444. doi:10.1016/j.jhazmat.2020.122444

Zhang, X., Li, Y., and Wang, Z. (2024). Enhanced thermal stability of high-purity silica for hightemperature applications. *J. Mater. Sci. Enginee.* 12(3), 456–470. doi:10.1016/j.jmat.2024.03.015

Zhang, X., Wang, H., Li, Y., Chen, Y., and Liu, Z. (2014). Removal of heavy metals from aqueous solution using nanostructured silica derived from rice husk ash. *J. Environ. Sci.* 26 (6), 1179–1186.

Zhang, Y. W. L. and. W. X. (2012). Synthesis of nanostructured silica from clay minerals: a review. *Appl. Clay Sci.* 67-68, 1–7. doi:10.1016/j.clay.2012.07.002

Zhang, Z. (2021). Sustainable production of silica for industrial applications: opportunities and challenges. *J. Clean. Prod.* 272, 122–134. doi:10.1016/j.jclepro.2020.122134

Zhang, Z., Liu, Y., Wang, X., Chen, J., Li, L., and Xu, G. (2020). Nanostructured silica: properties, synthesis, and applications. *J. Mater. Sci.* 55 (11), 4612–4629. doi:10.1007/s10853-020-04347-0

Zhao, A. (2015a). Microwave-assisted synthesis of mesoporous silica nanoparticles for drug delivery. *Microporous Mesoporous Mater.* 218, 123–129. doi:10.1016/j.micromeso.2015.06.041

Zhao, Y. (2015b). Synthesis of nanostructured silica from diatomaceous earth and its application in environmental remediation. *J. Environ. Chem. Eng.* 3 (4), 2732–2739. doi:10.1016/j.jece.2015.09.028

Zhuravlev, L. T. (2000). The surface chemistry of amorphous silica. Zhuravlev model. *Colloids Surfaces A Physicochem. Eng. Aspects* 173 (1-3), 1–38. doi:10.1016/s0927-7757(00)00556-2